ACS OMEGA

Article

http://pubs.acs.org/journal/acsodf

Enhanced Photoluminescence of Solution-Exfoliated Transition Metal Dichalcogenides by Laser Etching

Mark A. Bissett,*[,†] Andrew G. Hattle,[‡] Alexander J. Marsden,[†] Ian A. Kinloch,[†] and Robert A. W. Dryfe[‡]

[†]School of Materials and [‡]School of Chemistry, University of Manchester, Oxford Road, M13 9PL Manchester, U.K.

Supporting Information

ABSTRACT: Using a conventional Raman experimental apparatus, we demonstrate that the photoluminescent (PL) yield from ultrasonication-exfoliated transition metal dichalcogenides (TMDs) (MoS_2 and WS_2) can be increased by up to 8-fold by means of a laser etching procedure. This laser etching process allows us to controllably pattern and reduce the number of layers of the solution-exfoliated material, overcoming the key drawback to solvent-based exfoliation of two-dimensional (2D) semiconducting materials for applications in optoelectronics. The successful laser thinning of the exfoliated 2D crystals was investigated systematically by changes in both Raman and PL spectra. A simple proof-of-principle of the scalability of this laser etching technique for solution-exfoliated TMD crystals was also demonstrated. As well as being applicable for individual materials, it is also possible to use this simple laser etching technique to investigate the structure of solution-generated van der Waals heterostructures, consisting of layers of both MoS_2 and WS_2.

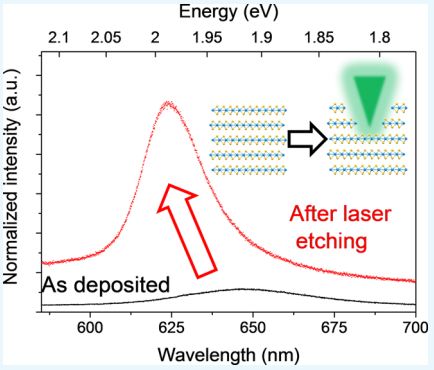

INTRODUCTION

Research into two-dimensional (2D) materials has continued to gain interest, first with graphene and then with other layered materials, such as the semiconducting transition metal dichalcogenides (TMDs), molybdenum disulfide (MoS_2), and tungsten disulfide (WS_2).[1−4] TMDs are of particular interest due to their unique electronic structure, and they exhibit a significant change in the band structure when reduced in thickness from bulk (indirect gap) to a monolayer (direct gap).[5−7] The transition to a direct gap semiconductor means that photons with an energy equal to the band gap can be easily absorbed or emitted, whereas the indirect band gap material requires an additional phonon absorption or emission to compensate for the difference in the momentum, making absorption much less efficient.[8] This change in electronic structure can typically be experimentally detected by a large increase in the photoluminescent (PL) quantum yield due to the increased efficiency of the direct band gap monolayer material.[9,10] This unique optical property is particularly important for photonic and optoelectronic applications including photovoltaics, light-emitting diodes, photodetectors, and displays.[6,7,11] Because of the atomically thin nature, it may also be possible to develop flexible and transparent optoelectronics.

Exfoliated monolayer TMDs can be produced by several methods including micromechanical exfoliation,[1] chemical vapor deposition (CVD),[12−14] chemical exfoliation,[15] electrochemical lithium intercalation,[16−18] and solvent-assisted ultrasonication.[19,20] Mechanical exfoliation produces the highest-quality crystals, with lateral dimensions of over 50 μm possible; however, the method is expensive, time consuming, and cannot be easily scaled for commercial applications. CVD growth can also produce high-quality large-area films of TMDs and can be scaled with continued progress, but it is also expensive and requires high temperatures for the growth, which limits the available substrates. Solvent exfoliation by ultrasonication, in contrast, is the only current method for economical production of large volumes of dispersed TMD sheets; however, the biggest drawback to solvent exfoliation is the reduced quality of the subsequent flakes due to the small lateral size, residual solvent, and a low monolayer content. Because of the low monolayer content, combined with the effect of contamination from the residual solvent molecules, very few studies have reported the PL response from ultrasonically exfoliated TMD flakes. To increase the applicability of the ultrasonic production method for use in optoelectronic applications, some form of post-processing is required to tune the layered structure.

It has previously been demonstrated that both mechanically exfoliated[21] and CVD-grown films[22,23] of MoS_2 can be thinned by laser etching in a controllable and reproducible manner using a simple laser setup, allowing for control over the number of layers as well as patterning into desired shapes. A similar process of laser etching has also previously been applied to other 2D materials such as graphene[24] and black phosphorus.[25,26] However, its application to solution-exfoliated TMDs would allow for a truly scalable production of efficient

Received: October 6, 2016
Accepted: December 26, 2016
Published: February 28, 2017

DOI: 10.1021/acsomega.6b00294
ACS Omega 2017, 2, 738−745

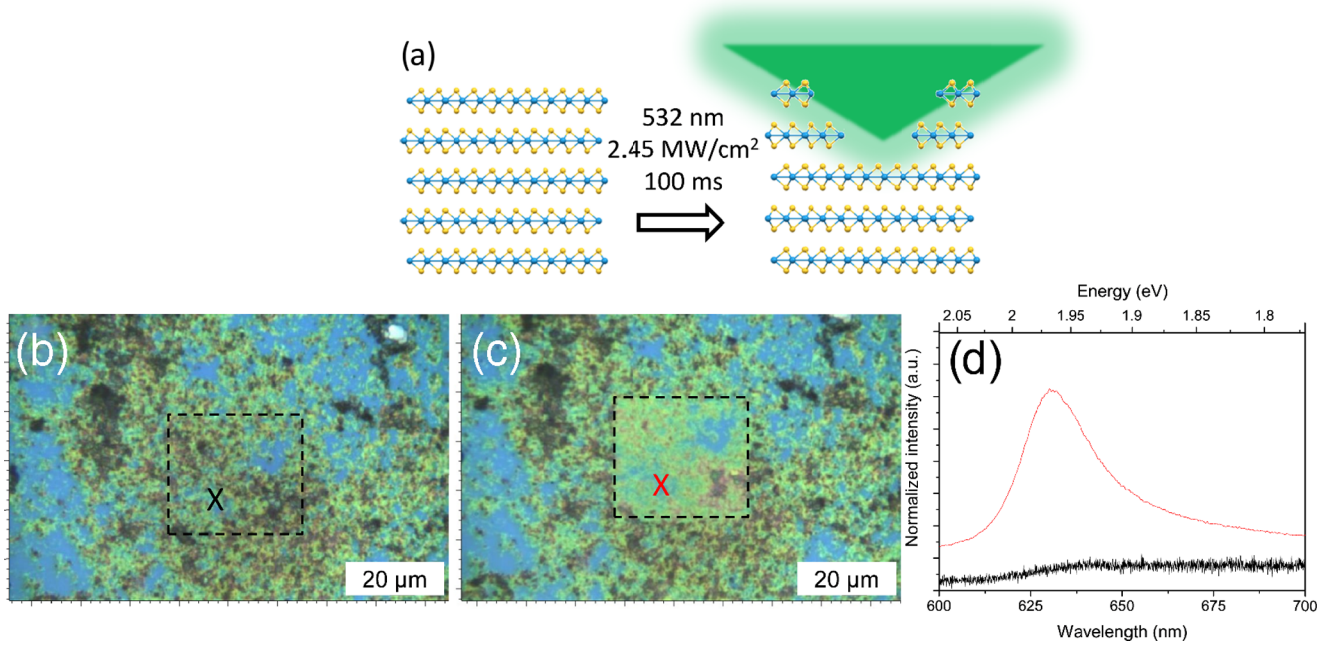

Figure 1. (a) Schematic showing the laser etching of an assembled stack of solution-exfoliated TMD layers. (b–c) Optical images showing a patch of agglomerated WS_2 flakes deposited on a SiO_2 wafer; the area marked by the box shows the obvious change in thickness, and consequently optical contrast after laser etching is performed. (d) PL spectra of the same area before (black) and after (red) laser etching showing the significant increase in signal intensity.

optoelectronic devices. The use of a laser etching process to perform the thinning and patterning of the sample has the benefit of avoiding the need for chemical photoresists or masks that can contaminate the flakes and alter the electronic structure. The mechanism behind the etching has been attributed to thermal sublimation of the upper TMD layers, with the heat being poorly dissipated through the structure due to weak van der Waals cohesive forces.[21,22] Because of this heat sink effect, the bottommost lasers directly in contact with the Si/SiO_2 wafer become increasingly difficult to remove and require an increased laser dosage when the laser irradiation is performed under ambient conditions. In addition to thermal sublimation of the crystals, there have been some reports of partial oxidation of the material (e.g., conversion of MoS_2 into MoO_3) due to the etching being performed under ambient conditions.[22] Chemical doping can also occur due to the freshly etched TMD layers being exposed to ambient atmospheric conditions (e.g., O_2, H_2O, and N_2). Previously, it has been observed that laser irradiation under ambient conditions leads to oxygen and water doping of the MoS_2 film and subsequent improvement of the photocurrent response.[22] Doping of the n-type semiconducting TMDs (e.g., MoS_2 and WS_2) by exposure to atmospherics molecules, such as O_2 and H_2O, is known to contribute to the enhancement of the PL intensity due to electron withdrawal by the dopant molecules stabilizing excitons and providing a new radiative recombination pathway.[27,28] This combined effect of chemical doping and morphological thinning can lead to an effective engineering of the electronic structure as well as providing tuning of the thickness.[29] This is of particular importance as chemical doping can be used to effectively tune the optoelectronic properties of the exfoliated flakes.

Heterostructures of different semiconducting 2D materials are also of great interest because of the ability to modify the electronic structure, thus introducing novel properties, and because of the fundamental interactions between each of the layers stacked together by van der Waals forces.[30−32] Owing to the close interaction between each of the exfoliated layers, it is possible for excited electrons and holes to transfer between the respective layers. These heterostructures have been demonstrated experimentally using mechanically exfoliated flakes manually stacked on top of one another;[33−35] however, this process is time consuming and lacks scalability. In addition to manual stacking, CVD-grown films grown on top of one another have been realized;[36−38] this technique shows promise but remains difficult to control and has a limited number of suitable growth substrates.

Here, we demonstrate that the PL intensity of solvent-exfoliated dispersions of both MoS_2 and the similarly structured WS_2 can be significantly increased (up to 8×), overcoming the key drawback of solvent-based exfoliation for applications in optoelectronics, by reducing the number of layers in a scalable manner. The optical properties of the flakes before and after etching are thoroughly characterized using Raman and PL spectroscopy, and the morphology of the flakes is analyzed using scanning electron microscopy (SEM). The laser etching of the solution-exfoliated TMD flakes is easily scalable as demonstrated over an arbitrary 250 μm × 250 μm area and can be applied to a wide variety of similarly structured 2D layered materials. We also investigate the properties of mixed dispersions of exfoliated MoS_2 and WS_2 flakes to create heterostructures. After depositing onto a silicon substrate, mixed heterostructures consisting of randomly stacked MoS_2 and WS_2 flakes are formed with differing thicknesses and stacking orders. The resultant stacks can then be modified through the use of laser etching, and the resultant 3D layered structure can be characterized.

DOI: 10.1021/acsomega.6b00294
ACS Omega 2017, 2, 738−745

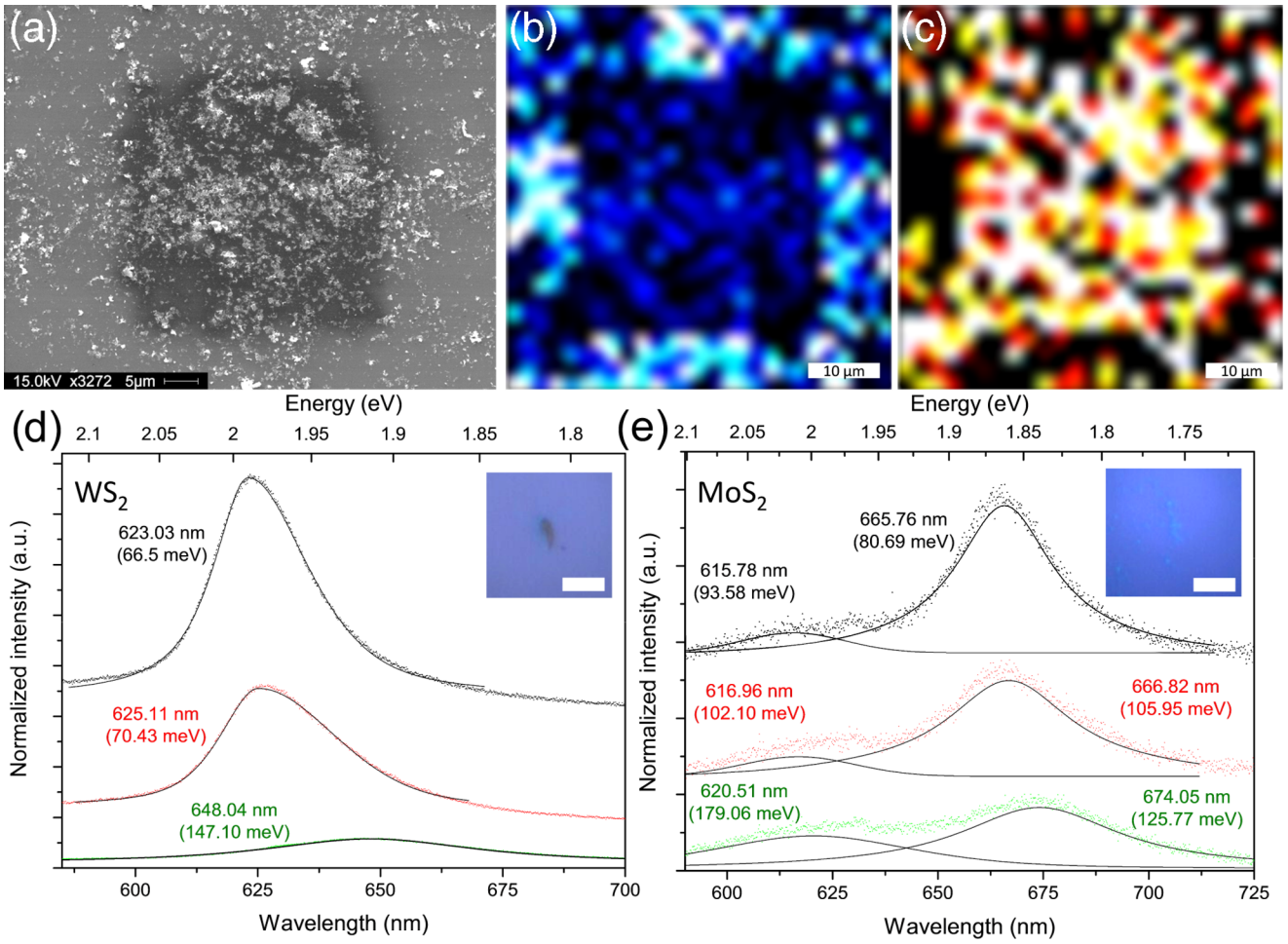

Figure 2. (a) SEM image showing deposited WS_2 nanoflakes after laser etching of a 20 μm × 20 μm area. (b) Map showing the Raman intensity of the WS_2 E_{2g} intensity over the same area showing the reduced signal intensity where etching has occurred. (c) Map showing the normalized PL intensity of the same area where the increased signal from inside the etched area is visible. PL spectra of the WS_2 (d) and MoS_2 (e) flakes with repeated laser etching. The as-deposited flakes are shown in green, followed by one cycle of laser etching in red and a second cycle of laser etching in black. The spectra in each figure are fitted with Lorentzian components, with the peak center labeled along with the full width at half-maximum (fwhm) (meV) in parentheses. The peak intensity has been normalized to the intensity of the Raman A_{1g} peak in each case. Insets show the optical image of the individual flakes before laser etching; the scale bar in each inset is 2 μm.

RESULTS AND DISCUSSION

After the formation of solvent-stabilized dispersions, the TMD flakes can then be deposited onto Si/SiO_2 wafers to act as a supporting substrate. The deposited flakes can form aggregates with lateral sizes of several microns, as seen in the typical optical image of the WS_2 flakes in Figure 1b, wherein repeated deposition was used to ensure that large-scale aggregates were clearly visible. A confocal Raman setup was used as both the etching laser source and the characterization tool, allowing rapid characterization of the same areas before and after etching. Etching was achieved by rastering the laser with a high incident power density over a designated area as seen schematically in Figure 1a. By controlling the exposure time, laser power, and scanning over designated areas in repeated cycles, it was possible to etch away the TMD flakes. After etching there is a clear change in the optical contrast of the deposited flakes, as seen in Figure 1c, indicating a reduction in the thickness of the flakes, and this can be used to approximate the thickness of the flakes.[39] When we compare the PL spectrum of the aggregated flakes before etching to that of the same area after the laser etching, as seen in Figure 1d, we see that there is a significant improvement in the signal intensity due to the reduced thickness of the flakes. Because of the large variation in the initial thickness of the aggregated flakes, some areas are reduced in thickness more than others. This is due to the mechanism of the laser etching, as the incoming laser light is absorbed and converted to heat, and the poor interlayer coupling causes the uppermost layers to be sublimed. The thinner flakes are in better thermal contact with the underlying substrate and can more strongly resist the localized heating.[21,40] Thus, the rate of etching is more pronounced on the thicker flakes compared to that of the thinner flakes for an equal exposure time.

After the ultrasonic exfoliation, the average MoS_2 and WS_2 flake dimensions are on the order of 200−300 nm, making them smaller than the size of the laser spot (~1 μm); this increases the exposure of the more reactive edges to the laser and may lead to the selective removal of highly defective edge structures. A similar effect has been observed previously for graphene films, which showed that, contrary to expectations, after laser etching the defect-related D band decreased in intensity due to selective removal of the highly reactive edges and defect sites.[24]

DOI: 10.1021/acsomega.6b00294
ACS Omega 2017, 2, 738−745

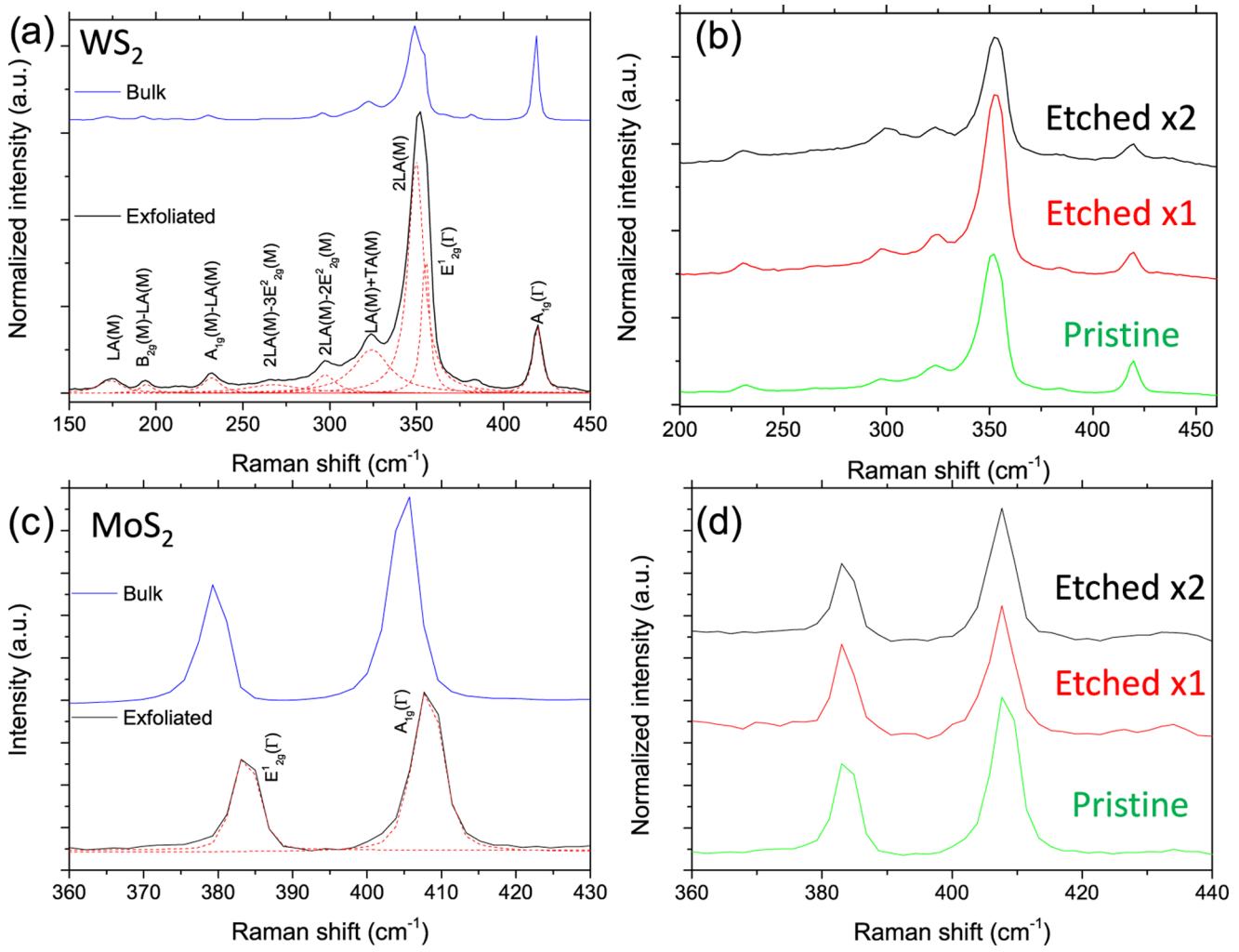

Figure 3. (a) Comparison of the Raman spectra of the bulk WS_2 powder (blue) and the solution-exfoliated WS_2 flakes (black) after deposition onto SiO_2, along with Lorentzian fitting and labeling according to literature peak assignments.[44] (b) Raman spectra of the same WS_2 flake after repeated laser etching. The spectra are normalized to the intensity of the A_{1g} peak. (c) Comparison of the Raman spectra of the bulk MoS_2 powder (blue) and the solution-exfoliated MoS_2 flakes (black) after deposition onto SiO_2, along with Lorentzian fitting and labeling according to literature peak assignments.[47] (d) Raman spectra of the same MoS_2 flake after repeated laser etching. The spectra are normalized to the intensity of the A_{1g} peak.

To further investigate the applicability of this laser etching procedure on solution-exfoliated TMD flakes, a thick coating of exfoliated WS_2 was deposited onto a Si/SiO_2 wafer and laser etched before analysis. Figure 2a shows an SEM image of the WS_2 flakes aggregated on the substrate after laser etching. The area (~20 μm × 20 μm) where the laser was rastered is clearly noticeable, indicating that this technique can be applied to large-scale samples as well as individual nanocrystals with a size of several hundred nanometers. By measuring the Raman spectrum across every point over this area, we can create a map of the E_{2g} intensity and compare how this changes across the etched area, as seen in Figure 2b. Clearly, there is reduced signal intensity from inside the laser-etched area, indicating the reduced thickness of the flakes. Interestingly, no peaks associated with tungsten oxides, WO_3[41] (or molybdenum oxide, MoO_3, in the case of MoS_2), were observed for the thin flakes, indicating that the etching process does not destroy the WS_2 or MoS_2 structure. However, in some areas of the thicker flakes, oxide peaks were occasionally detected (see Figure S2). The PL intensity was also mapped across the etched area, as seen in Figure 2c, and we see again an increased signal intensity within the etched areas. These results demonstrate that laser etching of solution-exfoliated TMDs can be performed over a designated area of an arbitrary size.

To further investigate this systematically, low-concentration dispersions were used to create small aggregates that were etched repeatedly, and the PL spectra were measured. The PL spectrum, normalized to the height of the A_{1g} Raman peak, of both the solution-exfoliated WS_2 and MoS_2 flakes, after dilution and deposition onto a silicon wafer, are shown in green in Figure 2d. Optical images showing the individual flakes as opposed to the large-scale aggregates are shown in the insets. The monolayer WS_2 PL emission typically contains a single peak, originating from the A exciton at ~1.95 eV.[8,42] The as-deposited WS_2 flakes shown in Figure 2d show a single low-intensity peak in the PL spectrum centered at 648 nm (1.91 eV), which corresponds to the energy expected for an approximately three-layer-thick WS_2 flake.[42] The fwhm of the PL peak can also provide information regarding the electronic structure of the TMD flakes. Typically, the fwhm of monolayer WS_2 is ~50−75 meV and that of MoS_2 is ~90 meV.[8,27,42,43] However, this value can vary depending on the doping of the flake and the localized strain or defects. The calculated fwhm (in meV) is shown in parentheses in Figure 2d,e for both the

DOI: 10.1021/acsomega.6b00294
ACS Omega 2017, 2, 738−745

WS_2 and the MoS_2 flakes. For the as-deposited WS_2 flakes (shown in green, Figure 2d), the fwhm is much larger than expected for the monolayer at ∼150 meV, again indicative of ∼3−5 layers. However, after laser etching of the WS_2 flakes there is a significant change in the PL response. After the first cycle of laser etching (shown in red), we notice a significant increase in the PL intensity, as may be expected due to the combination of reduced flake thickness combined with chemical doping by freshly exposing the etched surface to an ambient atmosphere, as mentioned previously.[27] The increase in the PL intensity after the first laser-etching cycle is by a factor of 5, and after repeated etching (shown in black), it increases further by a factor of 8 compared to that of the as-deposited flakes. This is a significant increase in the photoresponse of the solution-exfoliated flakes and could be valuable for use in applications in which the solution-exfoliated WS_2 flakes can be mass-produced and easily deposited as films on surfaces, followed by laser etching to increase the photoresponse as demonstrated previously for CVD-grown films.[22] As mentioned previously, as the laser etching removes the topmost WS_2 layers, it freshly exposes the underlying layer, providing a highly reactive surface that is rapidly passivated by atmospheric oxygen and water; these dopants increase the free carrier concentration of the WS_2 flakes, which can also increase the PL intensity. The width of the peaks also narrows significantly with laser etching, decreasing from ∼150 meV for the as-deposited flakes, to ∼70 meV after the first etching cycle, and finally to ∼66 meV after the second etching cycle, in agreement with the reduced number of layers and indicating the high quality of the thinned flakes.

To verify that the laser etching treatment is indeed reducing the thickness of the flakes, atomic force microscopy (AFM) was used to statistically measure the thickness of a number of individual WS_2 flakes before and after laser etching (see Figure S3). These flakes were prepared in the identical manner as described previously and deposited onto Si/SiO_2 wafers for analysis. It was found that after a single cycle of laser etching the average thickness of the flakes was decreased significantly, in agreement with the spectroscopic results. Also noticeable was the exposure of terrace-like structures within the thicker flakes. This indicates that the etching mechanism removes the uppermost layers preferentially before the lower layers.

A similar trend in PL response is observed for the MoS_2 flake, as seen in Figure 2e. Initially, the as-deposited MoS_2 flakes, shown in green, consist of two separate peaks referred to as the A and B excitons.[9,10] Similar to the WS_2 flakes, the as-deposited PL response of the solution-exfoliated MoS_2 exhibits a low intensity and very broad peaks, due to the thickness of the aggregated flakes. The literature values for the PL response for the monolayer MoS_2 flakes are 670 nm (∼1.85 eV) for the A exciton and 620 nm (∼2.00 eV) separated by ∼145 meV due to spin−orbit band splitting.[5,9,10,15] The PL response of the as-deposited flakes in Figure 2e matches fairly closely to the expected peak positions. After laser etching, the PL response of the MoS_2 flakes increases in intensity and narrows in width, indicating the reduced thickness of the flakes. After etching, the PL intensity increases initially by a factor of 1.5 and then by a factor of 2 compared to that of the as-deposited flakes. This is a lower enhancement of the PL intensity when compared to that of the WS_2 flakes and indicates that the PL enhancement is more effective in the case of the WS_2 flakes. This may also be related to the lower inherent PL intensity achieved by the MoS_2 flakes compared to that by the WS_2 flakes, making it more difficult to resolve the effects of atmospheric doping.

To systematically analyze the etching process on the solvent-exfoliated flakes, we can also look at the changes to the Raman spectra. Figure 3 shows the Raman spectra of the bulk powder and the solution-exfoliated WS_2 (a, b) and MoS_2 (c, d) flakes deposited onto the SiO_2 wafers after solvent removal. Low-concentration dispersions were used to minimize aggregation and allow the investigation of individual flakes. In Figure 3a, the Raman spectrum of WS_2 is shown with each of the peaks fitted with Lorentzian curves and labeled on the basis of literature peak assignments. The most significant peaks are the first-order A_{1g} (out-of-plane phonon) and E^1_{2g} (in-plane phonon) peaks that have been studied in detail previously; we also observe a rich variety of second-order peaks of WS_2, which are labeled according to the literature.[44] When we compare the spectrum of the bulk crystal to that of the solution-exfoliated flakes, we can immediately see a large difference in the intensity ratio of the A_{1g} and the overlapping E^1_{2g} and 2LA peaks. This intensity ratio can be used to determine the number of WS_2 layers present in the sample, as this ratio increases as the flakes are reduced in thickness.[44,45] In the spectra shown in Figure 3a, the $I_{2LA}/I_{A_{1g}}$ ratio is 0.8 for the bulk sample, whereas it is 3.4 for the exfoliated flake, indicating the few-layered (∼2−3) structure. With continued laser-etching cycles the amount of material is reduced, and this leads to a decrease in the signal intensity after each cycle. Thus, the spectra shown have been normalized to the intensity of the A_{1g} peak to allow for easy comparison. Figure 3b shows the Raman spectra of the as-deposited ultrasonication-exfoliated WS_2 flake, as well as after successive cycles of laser etching. When we compare the frequency of the Raman peaks after etching, we see very little shift in the peak position; however, we do see a change in the $I_{2LA}/I_{A_{1g}}$ ratio with continued etching. After the first etching cycle, the $I_{2LA}/I_{A_{1g}}$ ratio increases significantly to 5.1, and with the next etching cycle it increases slightly more to 5.2, indicating the reduced thickness of the deposited WS_2 flakes.

Figure 3c shows the comparison between the Raman spectrum of the bulk MoS_2 powder and the subsequent exfoliated flake, with the A_{1g} and E^1_{2g} phonon peaks labeled. We see a significant shift in the peak frequency when we compare the spectra before and after exfoliation, and this matches previous observations for similarly produced solution-exfoliated flakes.[46] This shift in phonon frequency is caused by the reduction in the number of layers of the MoS_2 and can be used to determine the thickness of the exfoliated flakes.[47,48] As seen in the case of WS_2, the as-deposited exfoliated MoS_2 flakes are predominantly few layered (∼2−3 layers), as expected from literature based on the sonication time and the centrifuge conditions used.[49] Figure 3d shows the Raman spectra of an as-deposited MoS_2 flake with repeated laser etching, similar to the WS_2 flake, seen previously. These spectra were obtained in the same $x-y$ position after etching to ensure that the same flake was being analyzed. Again there is very little noticeable shift in the position of the peaks with continued laser etching. However, although the shift in the Raman frequency is only minor for both the WS_2 and the MoS_2 flakes, we do see a significant change in the PL spectra after the laser etching as discussed previously.

As discussed previously, there is also a great deal of interest in the formation of vertically stacked van der Waals heterostructures, due to the unique electronic structure that

DOI: 10.1021/acsomega.6b00294
ACS Omega 2017, 2, 738−745

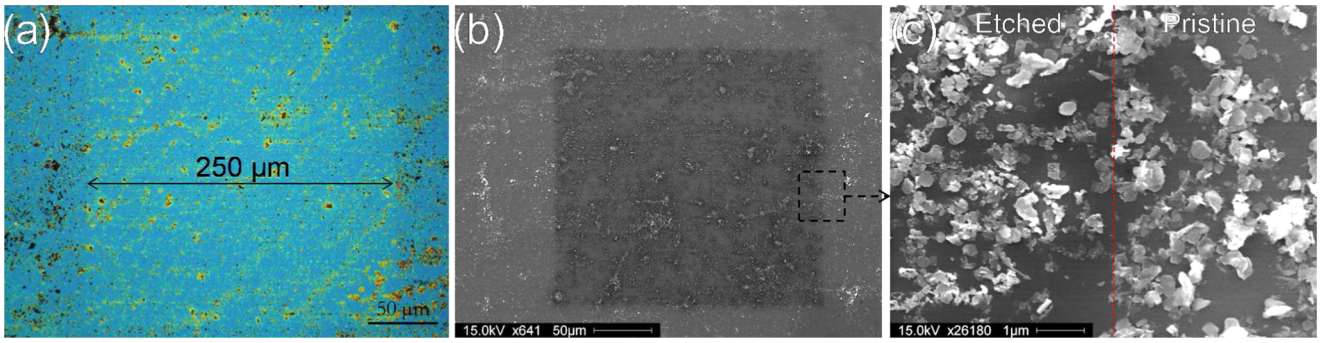

Figure 4. (a) Optical image of large-scale (250 μm × 250 μm) laser etching performed on the solution-exfoliated WS_2 flakes deposited onto a Si/SiO_2 wafer. (b) SEM image showing the same patterned area. (c) Increased magnification image showing the interface between the laser-etched and pristine deposited WS_2 flakes.

can be formed through the nonradiative transfer of excitons within each layer.[30−32,34−38] By creating these heterostructures by solution exfoliation, the interaction between the two materials can be analyzed easily. To investigate these heterostructures, dispersions of both exfoliated MoS_2 and WS_2 nanocrystals were mixed together and deposited onto substrates to create a series of heterostructures with random interlayer stacking as discussed in further detail in the Supporting Information (Figure S3).

LARGE-SCALE ETCHING

The key benefits of using solvent-based exfoliation over the previously demonstrated mechanical exfoliation and CVD growth of TMDs include both the low cost and the simple scalability. By creating large volumes of solvent-stabilized flakes and subsequently drop-casting or spin-coating them onto desired substrates, it is possible to demonstrate the large-scale applicability of this method. Previous examples showing a similar laser-etching process have only demonstrated this over comparatively small areas of several 10 s of micrometers due to sample size limitations.[21,22] In Figure 4, we demonstrate a proof-of-principle for the scalability of using liquid-exfoliated material by first simply drop-casting WS_2 flakes over a silicon wafer to create a large-scale coverage, which was then laser etched over a designated ∼250 μm × 250 μm area. Figure 4a shows the optical image of the etched area showing the distinct difference in optical contrast where the laser was rastered. Because of the use of simple drop-casting to deposit the flakes, there is a random assortment of thicknesses present on the surface; however, as the laser etching appears to more effectively remove thicker flakes due to poor thermal conductivity with the underlying substrate, repeated etching cycles can be used to produce an area of an approximately similar thickness. Figure 4b shows the SEM image of the same area where laser etching has occurred. In Figure 4c, an area of increased magnification shows the interface between the pristine as-deposited flakes and the laser-etched material, indicating a change in flake morphology. The selective etching of the crystal edges is also visible as the laser-etched flakes are seen to all have smoother edges than the pristine flakes as well as a reduced thickness. With further optimization, such as carefully controlling the initial concentration of the TMD dispersion and deposition conditions, it would be possible to create homogenous large-scale coatings that could then be post-processed using this laser-etching technique to enhance their mobility[21] and sensitivity to photons[22] or be patterned for further functionalization.[23,50]

EXPERIMENTAL SECTION

Dispersions of MoS_2 and WS_2 were produced following the established literature protocols.[19,49] Briefly, commercially available TMD powders (MoS_2 and WS_2) were each suspended in *N*-methylpyrrolidone (NMP) at a concentration of 10 mg mL^{-1}. To investigate the effect of the residual solvent, similar dispersions were also produced using a mixed solvent system of isopropanol (IPA) and water in a ratio of 7:3 (MoS_2) or 1:1 (WS_2) as this has previously been shown to match the exfoliation performance of NMP.[51,52] The suspension was then bath sonicated (Elmasonic P, 40% power, 37 kHz) for 12 h at a constant temperature of 20 °C. The resultant dispersion was then centrifuged at 6000 rpm (3139*g*) for 30 min, and the supernatant was decanted to provide a stable TMD dispersion. This technique has been shown to produce a distribution of flake sizes and thicknesses, ranging from a monolayer up to several layers (3−5) thick with lateral dimensions of 200−300 nm.[19,49] To characterize the flakes, the NMP suspension was first diluted by a factor of ∼50 in IPA to minimize the NMP and prevent agglomeration before drop-casting onto Si/SiO_2 wafers. The residual solvent was first evaporated on a hot plate at 50 °C before transferring into a vacuum oven and annealed at 200 °C at a pressure of 5 × 10^{-5} mbar to ensure thorough removal of the residual solvent. This vacuum annealing step was found to be vital in achieving the enhanced PL intensity after the laser etching, as without this step the residual solvent (NMP) molecules that are trapped between the TMD layers cause a large amount of amorphous carbon to appear in the Raman spectrum (seen in Figure S1). This amorphous carbon significantly suppresses the PL intensity of the MoS_2 or WS_2 flakes; however, after the vacuum annealing very little to no amorphous carbon was detected after the laser etching, indicating the successful removal of trapped solvent molecules and the increased cleanliness of the TMD flakes. In contrast, the IPA/H_2O dispersions were deposited as prepared onto the Si/SiO_2 wafers and left to dry, and little to no amorphous carbon was detected after etching.

Confocal Raman spectroscopy and PL measurements were conducted using a Renishaw inVia microscope with a 532 nm (2.33 eV) excitation at a power of 1.8 mW with a 100× objective and a grating of 1800 l/mm to achieve a spectral resolution of ∼1 cm^{-1}. Laser etching was performed using the same Raman setup, but with an incident laser power of ∼20 mW (power density: ∼2.45 MW cm^{-2}). The laser was rastered over a designated area in 500 nm steps with a typical exposure time of 100 ms per step, although this could be increased as

DOI: 10.1021/acsomega.6b00294
ACS Omega 2017, 2, 738−745

desired. For the large etching area, a lower magnification objective was used (20×), and a longer exposure time (~1 s) compensated for the lower power density. The morphology of the flakes after etching, as well as the individual crystal flake size of the TMDC materials, was characterized using a Philips/FEI XL30 FEG ESEM SEM. All images were obtained with an accelerating voltage of 15 kV, under high vacuum conditions utilizing secondary electron detection. AFM images were taken using a Bruker Multimode using the PeakForce Tapping mode under ambient conditions. After acquiring images of the pristine flakes, the sample was laser etched using the same conditions listed previously.

CONCLUSIONS

We have demonstrated that using a conventional Raman experimental setup it is possible to enhance the PL yield, by up to 8-fold, of ultrasonication-exfoliated MoS_2 and WS_2 using a simple laser-etching procedure. This laser-etching procedure, which had previously only been applied for mechanically exfoliated and CVD-grown MoS_2, has been demonstrated to be applicable for other solution-exfoliated 2D materials. The mechanism behind this PL improvement is a combination of the thinning of the material through thermal sublimation of the uppermost layers and atmospheric doping by H_2O and O_2 that occurs on the freshly exposed surface. This technique allows the cheap and scalable production of optoelectronic devices, which require the high quantum yield that monolayer flakes of these TMDs provide, while still using solution-based exfoliation. A simple proof-of-principle of the scalability of this laser-etching technique for solution-exfoliated TMD crystals was also demonstrated, indicating that there are many applications in which this would be beneficial, such as, photodetectors or other optoelectronics. Finally, this laser-etching technique was used to modify heterostructures (MoS_2 and WS_2) produced by mixing dispersions of each TMD, providing information about the structure and the ability to tune the optical properties as desired.

ASSOCIATED CONTENT

Supporting Information

The Supporting Information is available free of charge on the ACS Publications website at DOI: 10.1021/acsomega.6b00294.

Further Raman analysis of laser-etched samples; AFM analysis of pristine and laser-etched flakes; Raman and PL characterization of solution-phase-generated MoS_2/WS_2 heterostructures (PDF)

AUTHOR INFORMATION

Corresponding Author

*E-mail: Mark.Bissett@Manchester.ac.uk.

ORCID

Mark A. Bissett: 0000-0002-8908-7960

Robert A. W. Dryfe: 0000-0002-9335-4451

Author Contributions

The manuscript was written through contributions of all authors. All authors have given approval to the final version of the manuscript.

Notes

The authors declare no competing financial interest.

ACKNOWLEDGMENTS

The authors wish to thank the EPSRC for financial support (EP/J021229/1) under the auspices of the capital equipment funding for grid-scale energy storage.

REFERENCES

(1) Novoselov, K. S.; Jiang, D.; Schedin, F.; Booth, T. J.; Khotkevich, V. V.; Morozov, S. V.; Geim, A. K. Two-Dimensional Atomic Crystals. *Proc. Natl. Acad. Sci. U.S.A.* **2005**, *102*, 10451−10453.

(2) Koski, K. J.; Cui, Y. The New Skinny in Two-Dimensional Nanomaterials. *ACS Nano* **2013**, *7*, 3739−3743.

(3) Jariwala, D.; Sangwan, V. K.; Lauhon, L. J.; Marks, T. J.; Hersam, M. C. Emerging Device Applications for Semiconducting Two-Dimensional Transition Metal Dichalcogenides. *ACS Nano* **2014**, *8*, 1102−1120.

(4) Zhang, H. Ultrathin Two-Dimensional Nanomaterials. *ACS Nano* **2015**, *9*, 9451−9469.

(5) Ganatra, R.; Zhang, Q. Few-Layer Mos2: A Promising Layered Semiconductor. *ACS Nano* **2014**, *8*, 4074−4099.

(6) Zhao, W.; Ribeiro, R. M.; Eda, G. Electronic Structure and Optical Signatures of Semiconducting Transition Metal Dichalcogenide Nanosheets. *Acc. Chem. Res.* **2015**, *48*, 91−99.

(7) Li, H.; Wu, J.; Yin, Z.; Zhang, H. Preparation and Applications of Mechanically Exfoliated Single-Layer and Multilayer Mos2 and Wse2 Nanosheets. *Acc. Chem. Res.* **2014**, *47*, 1067−1075.

(8) Gutiérrez, H. R.; Perea-López, N.; Elías, A. L.; Berkdemir, A.; Wang, B.; Lv, R.; López-Urías, F.; Crespi, V. H.; Terrones, H.; Terrones, M. Extraordinary Room-Temperature Photoluminescence in Triangular Ws2 Monolayers. *Nano Lett.* **2013**, *13*, 3447−3454.

(9) Splendiani, A.; Sun, L.; Zhang, Y.; Li, T.; Kim, J.; Chim, C.-Y.; Galli, G.; Wang, F. Emerging Photoluminescence in Monolayer Mos_2. *Nano Lett.* **2010**, *10*, 1271−1275.

(10) Mak, K. F.; Lee, C.; Hone, J.; Shan, J.; Heinz, T. F. Atomically Thin Mos_2: A New Direct-Gap Semiconductor. *Phys. Rev. Lett.* **2010**, *105*, No. 136805.

(11) Wang, Q. H.; Kalantar-Zadeh, K.; Kis, A.; Coleman, J. N.; Strano, M. S. Electronics and Optoelectronics of Two-Dimensional Transition Metal Dichalcogenides. *Nat. Nanotechnol.* **2012**, *7*, 699−712.

(12) Wang, X.; Feng, H.; Wu, Y.; Jiao, L. Controlled Synthesis of Highly Crystalline Mos_2 Flakes by Chemical Vapor Deposition. *J. Am. Chem. Soc.* **2013**, *135*, 5304−5307.

(13) Cong, C.; Shang, J.; Wu, X.; Cao, B.; Peimyoo, N.; Qiu, C.; Sun, L.; Yu, T. Synthesis and Optical Properties of Large-Area Single-Crystalline 2d Semiconductor Ws2 Monolayer from Chemical Vapor Deposition. *Adv. Opt. Mater.* **2014**, *2*, 131−136.

(14) Kang, K.; Xie, S.; Huang, L.; Han, Y.; Huang, P. Y.; Mak, K. F.; Kim, C.-J.; Muller, D.; Park, J. High-Mobility Three-Atom-Thick Semiconducting Films with Wafer-Scale Homogeneity. *Nature* **2015**, *520*, 656−660.

(15) Eda, G.; Yamaguchi, H.; Voiry, D.; Fujita, T.; Chen, M.; Chhowalla, M. Photoluminescence from Chemically Exfoliated Mos_2. *Nano Lett.* **2011**, *11*, 5111−5116.

(16) Joensen, P.; Frindt, R. F.; Morrison, S. R. Single-Layer Mos_2. *Mater. Res. Bull.* **1986**, *21*, 457−461.

(17) Ramakrishna Matte, H. S. S.; Gomathi, A.; Manna, A. K.; Late, D. J.; Datta, R.; Pati, S. K.; Rao, C. N. R. Mos2 and Ws2 Analogues of Graphene. *Angew. Chem.* **2010**, *122*, 4153−4156.

(18) Zeng, Z.; Sun, T.; Zhu, J.; Huang, X.; Yin, Z.; Lu, G.; Fan, Z.; Yan, Q.; Hng, H. H.; Zhang, H. An Effective Method for the Fabrication of Few-Layer-Thick Inorganic Nanosheets. *Angew. Chem., Int. Ed.* **2012**, *51*, 9052−9056.

(19) Coleman, J. N.; et al. Two-Dimensional Nanosheets Produced by Liquid Exfoliation of Layered Materials. *Science* **2011**, *331*, 568−571.

(20) Nicolosi, V.; Chhowalla, M.; Kanatzidis, M. G.; Strano, M. S.; Coleman, J. N. Liquid Exfoliation of Layered Materials. *Science* **2013**, *340*, No. 1226419.

DOI: 10.1021/acsomega.6b00294
ACS Omega 2017, 2, 738−745

(21) Castellanos-Gomez, A.; Barkelid, M.; Goossens, A. M.; Calado, V. E.; van der Zant, H. S. J.; Steele, G. A. Laser-Thinning of Mos2: On Demand Generation of a Single-Layer Semiconductor. *Nano Lett.* **2012**, *12*, 3187−3192.
(22) Lu, J.; Lu, J. H.; Liu, H.; Liu, B.; Chan, K. X.; Lin, J.; Chen, W.; Loh, K. P.; Sow, C. H. Improved Photoelectrical Properties of Mos2 Films after Laser Micromachining. *ACS Nano* **2014**, *8*, 6334−6343.
(23) Lu, J.; Lu, J. H.; Liu, H.; Liu, B.; Gong, L.; Tok, E. S.; Loh, K. P.; Sow, C. H. Microlandscaping of Au Nanoparticles on Few-Layer Mos_2 Films for Chemical Sensing. *Small* **2015**, *11*, 1792−1800.
(24) Del, S. K.; Bornemann, R.; Bablich, A.; Schäfer-Eberwein, H.; Li, J.; Kowald, T.; Östling, M.; Bolívar, P. H.; Lemme, M. C. Optimizing the Optical and Electrical Properties of Graphene Ink Thin Films by Laser-Annealing. *2D Mater.* **2015**, *2*, No. 011003.
(25) Lu, J.; Wu, J.; Carvalho, A.; Ziletti, A.; Liu, H.; Tan, J.; Chen, Y.; Castro Neto, A. H.; Özyilmaz, B.; Sow, C. H. Bandgap Engineering of Phosphorene by Laser Oxidation toward Functional 2d Materials. *ACS Nano* **2015**, *9*, 10411−10421.
(26) Lu, J.; Carvalho, A.; Wu, J.; Liu, H.; Tok, E. S.; Neto, A. H. C.; Özyilmaz, B.; Sow, C. H. Enhanced Photoresponse from Phosphorene−Phosphorene-Suboxide Junction Fashioned by Focused Laser Micromachining. *Adv. Mater.* **2016**, *28*, 4090−4096.
(27) Tongay, S.; Zhou, J.; Ataca, C.; Liu, J.; Kang, J. S.; Matthews, T. S.; You, L.; Li, J.; Grossman, J. C.; Wu, J. Broad-Range Modulation of Light Emission in Two-Dimensional Semiconductors by Molecular Physisorption Gating. *Nano Lett.* **2013**, *13*, 2831−2836.
(28) Nan, H.; et al. Strong Photoluminescence Enhancement of Mos2 through Defect Engineering and Oxygen Bonding. *ACS Nano* **2014**, *8*, 5738−5745.
(29) Lu, J.; Carvalho, A.; Chan, X. K.; Liu, H.; Liu, B.; Tok, E. S.; Loh, K. P.; Castro Neto, A. H.; Sow, C. H. Atomic Healing of Defects in Transition Metal Dichalcogenides. *Nano Lett.* **2015**, *15*, 3524−3532.
(30) Lim, H.; Yoon, S. I.; Kim, G.; Jang, A. R.; Shin, H. S. Stacking of Two-Dimensional Materials in Lateral and Vertical Directions. *Chem. Mater.* **2014**, *26*, 4891−4903.
(31) Geim, A. K.; Grigorieva, I. V. Van Der Waals Heterostructures. *Nature* **2013**, *499*, 419−425.
(32) Zhu, X.; Monahan, N. R.; Gong, Z.; Zhu, H.; Williams, K. W.; Nelson, C. A. Charge Transfer Excitons at Van Der Waals Interfaces. *J. Am. Chem. Soc.* **2015**, *137*, 8313−8320.
(33) Lee, C.-H.; et al. Atomically Thin P−N Junctions with Van Der Waals Heterointerfaces. *Nat. Nanotechnol.* **2014**, *9*, 676−681.
(34) Ceballos, F.; Bellus, M. Z.; Chiu, H.-Y.; Zhao, H. Ultrafast Charge Separation and Indirect Exciton Formation in a Mos2−Mose2 Van Der Waals Heterostructure. *ACS Nano* **2014**, *8*, 12717−12724.
(35) Fang, H.; et al. Strong Interlayer Coupling in Van Der Waals Heterostructures Built from Single-Layer Chalcogenides. *Proc. Natl. Acad. Sci. U.S.A.* **2014**, *111*, 6198−6202.
(36) Gong, Y.; et al. Vertical and in-Plane Heterostructures from Ws2/Mos2 Monolayers. *Nat. Mater.* **2014**, *13*, 1135−1142.
(37) Hong, X.; Kim, J.; Shi, S.-F.; Zhang, Y.; Jin, C.; Sun, Y.; Tongay, S.; Wu, J.; Zhang, Y.; Wang, F. Ultrafast Charge Transfer in Atomically Thin Mos2/Ws2 Heterostructures. *Nat. Nanotechnol.* **2014**, *9*, 682−686.
(38) Huang, C.; Wu, S.; Sanchez, A. M.; Peters, J. J. P.; Beanland, R.; Ross, J. S.; Rivera, P.; Yao, W.; Cobden, D. H.; Xu, X. Lateral Heterojunctions within Monolayer Mose2−Wse2 Semiconductors. *Nat. Mater.* **2014**, *13*, 1096−1101.
(39) Castellanos-Gomez, A.; Agraït, N.; Rubio-Bollinger, G. Optical Identification of Atomically Thin Dichalcogenide Crystals. *Appl. Phys. Lett.* **2010**, *96*, No. 213116.
(40) Wu, J.; Li, H.; Yin, Z.; Li, H.; Liu, J.; Cao, X.; Zhang, Q.; Zhang, H. Layer Thinning and Etching of Mechanically Exfoliated Mos2 Nanosheets by Thermal Annealing in Air. *Small* **2013**, *9*, 3314−3319.
(41) Daniel, M. F.; Desbat, B.; Lassegues, J. C.; Gerand, B.; Figlarz, M. Infrared and Raman Study of Wo3 Tungsten Trioxides and Wo3, Xh2o Tungsten Trioxide Tydrates. *J. Solid State Chem.* **1987**, *67*, 235−247.
(42) Zhao, W.; Ghorannevis, Z.; Chu, L.; Toh, M.; Kloc, C.; Tan, P.-H.; Eda, G. Evolution of Electronic Structure in Atomically Thin Sheets of Ws2 and Wse2. *ACS Nano* **2013**, *7*, 791−797.
(43) Scheuschner, N.; Ochedowski, O.; Kaulitz, A.-M.; Gillen, R.; Schleberger, M.; Maultzsch, J. Photoluminescence of Freestanding Single- and Few-Layer Mos_2. *Phys. Rev. B* **2014**, *89*, No. 125406.
(44) Berkdemir, A.; et al. Identification of Individual and Few Layers of Ws2 Using Raman Spectroscopy. *Sci. Rep.* **2013**, *3*, 1755.
(45) Zhao, W.; Ghorannevis, Z.; Amara, K. K.; Pang, J. R.; Toh, M.; Zhang, X.; Kloc, C.; Tan, P. H.; Eda, G. Lattice Dynamics in Mono- and Few-Layer Sheets of Ws2 and Wse2. *Nanoscale* **2013**, *5*, 9677−9683.
(46) Bissett, M. A.; Kinloch, I. A.; Dryfe, R. A. W. Characterization of Mos_2-Graphene Composites for High-Performance Coin Cell Supercapacitors. *ACS Appl. Mater. Interfaces* **2015**, *7*, 17388−17398.
(47) Lee, C.; Yan, H.; Brus, L. E.; Heinz, T. F.; Hone, J.; Ryu, S. Anomalous Lattice Vibrations of Single- and Few-Layer Mos2. *ACS Nano* **2010**, *4*, 2695−2700.
(48) Li, H.; Zhang, Q.; Yap, C. C. R.; Tay, B. K.; Edwin, T. H. T.; Olivier, A.; Baillargeat, D. From Bulk to Monolayer Mos_2: Evolution of Raman Scattering. *Adv. Funct. Mater.* **2012**, *22*, 1385−1390.
(49) O'Neill, A.; Khan, U.; Coleman, J. N. Preparation of High Concentration Dispersions of Exfoliated Mos_2 with Increased Flake Size. *Chem. Mater.* **2012**, *24*, 2414−2421.
(50) Tran Khac, B. C.; Jeon, K.-J.; Choi, S. T.; Kim, Y. S.; DelRio, F. W.; Chung, K.-H. Laser-Induced Particle Adsorption on Atomically Thin Mos2. *ACS Appl. Mater. Interfaces* **2016**, *8*, 2974−2984.
(51) Shen, J.; et al. Liquid Phase Exfoliation of Two-Dimensional Materials by Directly Probing and Matching Surface Tension Components. *Nano Lett.* **2015**, *15*, 5449−5454.
(52) Shen, J.; et al. Surface Tension Components Based Selection of Cosolvents for Efficient Liquid Phase Exfoliation of 2d Materials. *Small* **2016**, *12*, 2741.

DOI: 10.1021/acsomega.6b00294
ACS Omega 2017, 2, 738−745